

Formation mechanism of chemically precompressed hydrogen clathrates in metal superhydrides

Shichang Yao, Chongze Wang, Shuyuan Liu, Hyunsoo Jeon, and Jun-Hyung Cho*

*Department of Physics, Research Institute for Natural Science,
and Institute for High Pressure at Hanyang University, Hanyang University,
222 Wangsimni-ro, Seongdong-Ku, Seoul 04763, Republic of Korea*

(Dated: October 7, 2021)

Recently, the experimental discovery of high- T_c superconductivity in compressed hydrides H_3S and LaH_{10} at megabar pressures has triggered searches for various superconducting superhydrides. It was experimentally observed that thorium hydrides, ThH_{10} and ThH_9 , are stabilized at much lower pressures compared to LaH_{10} . Based on first-principles density-functional theory calculations, we reveal that the isolated Th frameworks of ThH_{10} and ThH_9 have relatively more excess electrons in interstitial regions than the La framework of LaH_{10} . Such interstitial excess electrons easily participate in the formation of anionic H cage surrounding metal atom. The resulting Coulomb attraction between cationic Th atoms and anionic H cages is estimated to be stronger than the corresponding one of LaH_{10} , thereby giving rise to larger chemical precompressions in ThH_{10} and ThH_9 . Such a formation mechanism of H clathrates can also be applied to another experimentally synthesized superhydride CeH_9 , confirming the experimental evidence that the chemical precompression in CeH_9 is larger than that in LaH_{10} . Our findings demonstrate that interstitial excess electrons in the isolated metal frameworks of high-pressure superhydrides play an important role in generating the chemical precompression of H clathrates.

I. INTRODUCTION

In recent years, hydrides have attracted much attention theoretically and experimentally because of their promising possibility for the realization of room-temperature superconductivity (SC) [1, 2]. Motivated by the pioneering idea of Neil Ashcroft on high-temperature SC in metallic hydrogen [3] and the incessant theoretical predictions of high superconducting transition temperature T_c in a number of hydrides [4–20], experiments have confirmed that sulfur hydride H_3S and lanthanum hydride LaH_{10} exhibit T_c around 203 K at ~ 155 GPa [21] and 250–260 K at ~ 170 GPa [22, 23], respectively. Subsequently, such a conventional Bardeen-Cooper-Schrieffer type SC has also been experimentally observed in various compressed hydrides at high pressures [24–30]. For examples, ThH_{10} (ThH_9) exhibits $T_c = 159$ –161 (146) K between 170 and 175 GPa [24], while CeH_9 exhibits a T_c of ~ 100 K at 130 GPa [27]. More recently, carbonaceous sulfur hydride was observed to exhibit a room-temperature SC with a T_c of 288 K at ~ 267 GPa [30]. Therefore, the experimental observations of high-temperature SC in either surfur-containing hydrides [21, 30] or superhydrides containing an abnormally large amount of hydrogen [22–28] has launched a new era of high- T_c superconductors.

Compared to the existence of metallic hydrogen at high pressures over ~ 400 GPa [31, 32], the syntheses of superhydrides with H-rich clathrate structures have been achieved at relatively much lower pressures, because H atoms can be “chemically precompressed” by chemical forces between metal atoms and H cages [33]. Using density-functional theory (DFT) calculations, the high- T_c superconducting phases of various superhydrides have been predicted to be metastable at higher pressures than a critical pressure P_c [34–37]. It is noticeable that the magnitude of P_c reflects the strength of chemical precompression in superhydrides. Experimentally, the P_c value of ThH_{10} having a fcc-Th framework [see Fig. 1(a)] was measured to be ~ 85 GPa [24], much lower than $P_c \sim 170$ of an isostructural superhydride LaH_{10} [22, 23]. Fur-

thermore, ThH_9 (CeH_9) having a hcp metal framework [see Fig. 1(b)] was observed to exhibit a P_c of ~ 86 (80) GPa [24–27]. Based on these existing experimental data [22–24], it is most likely that P_c changes with respect to metal species: i.e., Group-4 metal hydrides ThH_{10} , ThH_9 , and CeH_9 with occupied f -subshell electrons have lower P_c values or larger chemical precompressions compared to a Group-3 metal hydride LaH_{10} . Our recent DFT calculations for LaH_{10} [38] revealed that the isolated La framework without H atoms behaves as an electride at high pressures, where some electrons detached from La atoms are well localized in interstitial regions. These interstitial excess electrons are easily captured to H atoms, forming a H clathrate structure in LaH_{10} . In the present study, such an electride feature in the La framework of LaH_{10} is compared with other metal frameworks of the above-mentioned superhydrides ThH_{10} , ThH_9 , and CeH_9 . By the estimation of Coulomb attractions between metal atoms and H cages, we provide an explanation for the different chemical precompressions observed in such superhydrides [22–27], as will be discussed below.

In this paper, using first-principles DFT calculations, we perform a comparative study of chemical precompressions in ThH_{10} , ThH_9 , CeH_9 , and LaH_{10} . We find that the isolated metal frameworks of ThH_{10} , ThH_9 , and CeH_9 possess more interstitial excess electrons than that of LaH_{10} at an equal pressure of 300 GPa. Such loosely bound electrons can be easily captured to form H clathrate structures with attractive Coulomb interactions between cationic metal atoms and anionic H cages. Using the calculated Bader charges [39] and positions of metal and H atoms in each superhydride, we estimate a chemical pressure acting on H cage around a metal atom. As a result, ThH_{10} , ThH_9 , and CeH_9 are found to have larger chemical precompressions than LaH_{10} , consistent with the experimentally observed P_c values in these superhydrides [22–27]. It is thus demonstrated that Group-4 metal hydrides occupying f electrons can be more chemically precompressed compared to Group-3 metal hydride, thereby contributing to lower P_c . The present findings illuminate that in-

terstitial excess electrons in the metal frameworks of superhydrides are of importance to generate the chemical precompression of H cages around metal atoms.

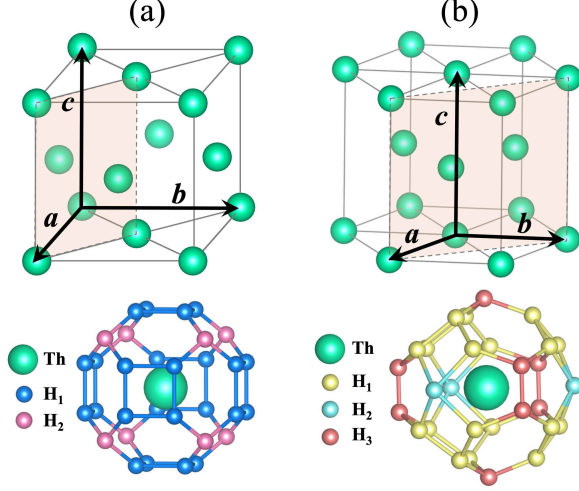


FIG. 1. Optimized structures of (a) ThH₁₀ and (b) ThH₉ at 300 GPa. ThH₁₀ (ThH₉) has the fcc (hcp) Th framework with the H₃₂ (H₂₉) cage surrounding each Th atom. There are two (three) different types of H atoms: i.e., H₁ and H₂ for ThH₁₀ (H₁, H₂, and H₃ for ThH₉). The (110) planes are drawn in the fcc and hcp lattices.

II. CALCULATIONAL METHODS

Our first-principles DFT calculations were performed using the Vienna *ab initio* simulation package with the projector-augmented wave method [40–42]. Here, we treated Th $6s^2 6p^6 5f^1 6d^1 7s^2$, Ce $5s^2 5p^6 4f^1 5d^1 6s^2$, La $5s^2 5p^6 5d^1 6s^2$ and H $1s^1$ as valence electrons, including $6s^2 6p^6$, $5s^2 5p^6$, and $5s^2 5p^6$ semicore electrons for Th, Ce, and La, respectively. For the exchange-correlation energy, we employed the generalized-gradient approximation functional of Perdew-Burke-Ernzerhof [43, 44]. A plane-wave basis was used with a kinetic energy cutoff of 500 eV for ThH₁₀ and ThH₉. The \mathbf{k} -space integration was done with $24 \times 24 \times 24$ and $18 \times 18 \times 12$ \mathbf{k} points for ThH₁₀ and ThH₉, respectively. All atoms were allowed to relax along the calculated forces until all the residual force components were less than 0.005 eV/Å. We calculated phonon frequencies with the $6 \times 6 \times 6$ ($5 \times 5 \times 3$) q points for ThH₁₀ (ThH₉) using the QUANTUM ESPRESSO package [45]. For CeH₉ and LaH₁₀, we chose the calculation parameters used in our previous works [38, 46].

III. RESULTS

We first optimize the structures of experimentally synthesized superhydrides ThH₁₀, ThH₉, CeH₉, and LaH₁₀ as a function of pressure using DFT calculations. These superhydrides have hydrogen sodalitelike clathrate structures with high-symmetry space groups: i.e., $Fm\bar{3}m$ (No. 225) for ThH₁₀

and LaH₁₀, while $P6_3/mmc$ (No. 194) for ThH₉ and CeH₉. As shown in Fig. 1(a), ThH₁₀ (LaH₁₀) is constituted by the fcc metal framework, where each Th (La) atom is surrounded by the H₃₂ cage consisting of 32 H atoms. Meanwhile, ThH₉ (CeH₉) have the hcp metal framework with the H₂₉ cage surrounding a Th (Ce) atom [see Fig. 1(b)]. Note that there are two (three) species of H atoms composing the H₃₂ (H₂₉) cages in ThH₁₀ and LaH₁₀ (ThH₉ and CeH₉). The optimized structures of these superhydrides show that the lattice constants decrease monotonously with increasing pressure (see Fig. S1 in the Supplemental Material). Accordingly, the averaged bond lengths d_{M-H} between metal and H atoms decrease with increasing pressure [see Fig. 2(a)]. We find that d_{M-H} for ThH₁₀ having the H₃₂ cage is longer than ThH₉ having the H₂₉ cage at a given pressure. Meanwhile, d_{M-H} for CeH₉ is shorter than that for ThH₉, possibly because of the smaller size of Ce atom with the atomic number of $Z = 58$ compared to Th atom with $Z = 90$. Interestingly, despite the larger atomic number of Th than La ($Z = 57$), the d_{M-H} values for ThH₁₀ and ThH₉ are close to that for LaH₁₀ at a given pressure, implying that the former superhydrides have larger chemical precompressions than the latter one. We note that the charges of cationic metal and anionic H atoms are also essential ingredients for determining chemical precompression, as discussed below. Figure 2(b) displays the averaged H–H bond lengths d_{H-H} for ThH₁₀, ThH₉, CeH₉, and LaH₁₀, which also decrease monotonously with increasing pressure. It is seen that the d_{H-H} values for ThH₁₀ and LaH₁₀ are shorter than those for ThH₉ and CeH₉, indicating that the H₃₂ cages composed of larger number of H atoms give rise to shorter d_{H-H} compared to the H₂₉ cages.

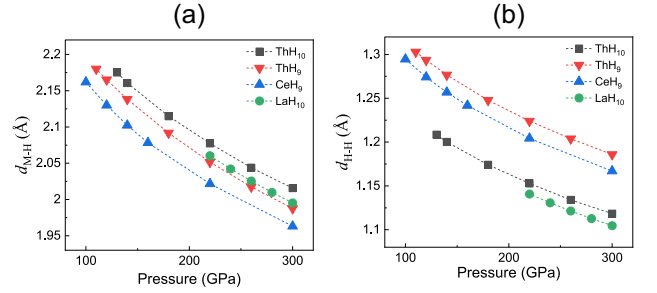


FIG. 2. Calculated averaged bond lengths (a) d_{M-H} between metal and H atoms and (b) d_{H-H} between H atoms for ThH₁₀, ThH₉, CeH₉, and LaH₁₀ as a function of pressure.

In order to examine the dynamical stability of ThH₁₀, ThH₉, CeH₉, and LaH₁₀, we calculate their phonon spectra as a function of pressure. As shown in Fig. 3(a), the phonon spectrum of ThH₁₀, calculated at 130 GPa, exhibits the softening of low-energy phonon modes (marked by arrows) along the $\Gamma-L$ and $\Gamma-K$ lines. Such H-derived phonon modes finally have imaginary frequencies at 120 GPa [see Fig. 3(b)]. This indicates that the fcc-ThH₁₀ phase becomes unstable as pressure decreases. Therefore, the phonon spectra as a function of pressure allow us to predict the P_c values of about 130, 110, 100, and 220 GPa for ThH₁₀, ThH₉, CeH₉ [46], and LaH₁₀ [36], respectively (see Fig. S2 in the Supplemental Ma-

terial). We find that ThH_{10} and ThH_9 have much lower P_c than LaH_{10} , while their P_c values are close to that of CeH_9 . The overall trend of these predicted P_c values in four superhydrides are well consistent with the experimentally measured ones of about 85, 86, 80, and 170 GPa for ThH_{10} [24], ThH_9 [24], CeH_9 [25–27], and LaH_{10} [22, 23], respectively. It was previously pointed out that for LaH_{10} , the anharmonic effects on phonons and the quantum ionic zero-point energy are of importance for a proper prediction of P_c [47]. Therefore, the above overestimation of predicted P_c values is likely due to the ignorance of anharmonic and quantum effects [48–50] in the present theory. Nevertheless, we can say that ThH_{10} , ThH_9 , and CeH_9 have significantly larger chemical precompressions compared to LaH_{10} .

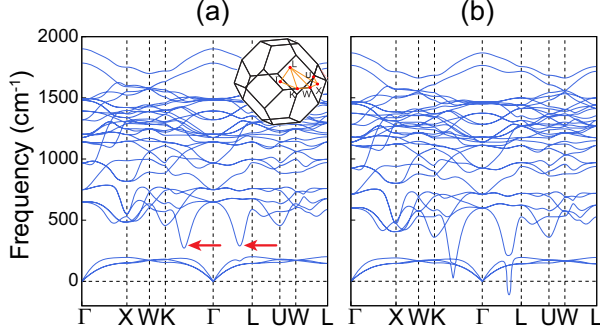


FIG. 3. Calculated phonon spectra of ThH_{10} at (a) 130 and (b) 120 GPa. The arrows in (a) indicate the softened phonon modes. The imaginary phonon frequencies appear at 120 GPa along the $\Gamma-L$ line.

We next explore the electrone-like characteristics of the isolated metal frameworks of ThH_{10} , ThH_9 , CeH_9 , and LaH_{10} . Here, the structure of each metal framework is taken from the optimized structure of the corresponding superhydride. The valence charge densities ρ_M (without including of semicore electrons) of the metal frameworks of ThH_{10} , ThH_9 , CeH_9 , and LaH_{10} , calculated at an equal pressure of 300 GPa, are displayed in Figs. 4(a), 4(c), 4(e), and 4(g), respectively. It is seen that some electrons detached from metal atoms are localized in the interstitial regions around the A_1 and A_2 sites. These interstitial excess electrons of the so-called A_1 and A_2 anions are well confirmed by the corresponding electron localization function (ELF) [51]. Figures. 4(b), 4(d), 4(f), and 4(h) represent the calculated ELF of the metal frameworks of ThH_{10} , ThH_9 , CeH_9 , and LaH_{10} , respectively. For the Th framework of ThH_{10} , the number of electrons Q_{A_1} (Q_{A_2}) within the muffin-tin sphere of the A_1 (A_2) anion is -0.281 (-0.234) e , larger in magnitude than -0.204 (-0.194) e for the La framework of LaH_{10} [see Figs. 4(a) and 4(g)]. Similarly, as shown in Figs. 4(c) and 4(e), Q_{A_1} (Q_{A_2}) in ThH_9 is -0.124 (-0.080) e , larger in magnitude than the corresponding value of -0.118 (-0.072) e in CeH_9 . Therefore, the metal framework of ThH_{10} (ThH_9) exhibits a more electrone-like feature than that of LaH_{10} (CeH_9). It is noted that the magnitudes of Q_{A_1} and Q_{A_2} change as a function of pressure (see Figs. S3 and S4 in the Supplemental Material), showing that the electrone-like characteristics of metal frameworks are enhanced with in-

creasing pressure. Indeed, the localization of interstitial excess electrons also emerges in compressed alkali metals at high pressures [52–54], in order to reduce Coulomb repulsions arising from the overlap of atomic valence electrons. Such loosely bound anionic electrons residing in the metal frameworks of compressed superhydrides can be easily captured to H atoms, forming H cages with attractive Coulomb interactions between cationic metal and anionic H atoms. It is remarkable that the anionic electrons in H cages are mostly supplied because of the electrone nature of metal frameworks at high pressures, rather than due to the different electronegativities of metal and H atoms [11].

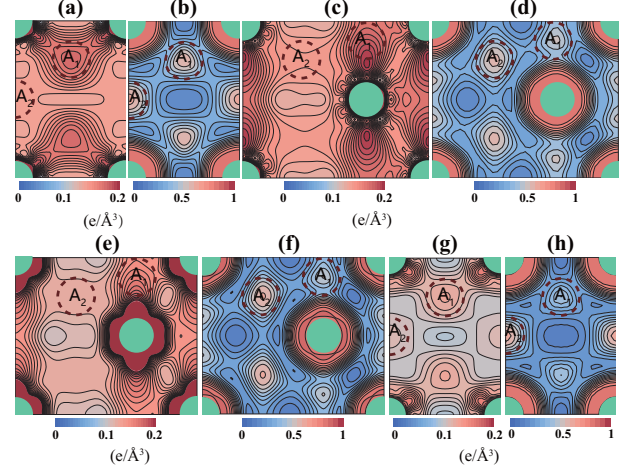


FIG. 4. Calculated valence charge density plot of the metal frameworks of (a) ThH_{10} , (c) ThH_9 , (e) CeH_9 , and (g) LaH_{10} at 300 GPa, together with the ELF of the metal frameworks of (b) ThH_{10} , (d) ThH_9 , (f) CeH_9 , and (h) LaH_{10} . The charge densities in (a), (c), (e), and (g) are drawn on the (110) plane with a contour spacing of $0.005 \text{ e}/\text{\AA}^3$. The ELF in (b), (d), (f), and (h) are drawn with a contour spacing of 0.05. A_1 and A_2 indicate the two anions in interstitial regions, and the dashed circles represent the muffin-tin spheres around A_1 and A_2 with the radii of 0.75 (0.60) and 0.75 (0.60) \AA in ThH_{10} and LaH_{10} (ThH_9 and CeH_9), respectively.

Figures 5(a) and 5(b) show the calculated total charge densities of ThH_{10} and ThH_9 at 300 GPa, respectively. It is seen that the H atoms in each H cage are bonded to each other with covalent bonds, where each H–H bond has a saddle point of charge density at its midpoint, similar to the C–C covalent bond in diamond [55]. For ThH_{10} (ThH_9), the charge densities $\rho_{\text{H-H}}$ at the midpoints of the H–H bonds are 0.911 and 0.729 (0.992, 0.769, and 0.601) $\text{e}/\text{\AA}^3$: see the arrows in Figs. 5(a) and 5(b). In order to confirm that the interstitial excess electrons of the Th framework of ThH_{10} (ThH_9) are captured to form the H_{32} (H_{29}) cages, we calculate the charge densities of the isolated H_{32} (H_{29}) cages without Th atoms. Here, the structure of each isolated H cage is taken from the optimized structure of the corresponding superhydride. As shown in Fig. 5(c) [5(d)], we find that $\rho_{\text{H-H}}$ decreases as 0.742 and 0.621 (0.843, 0.580, and 0.479) $\text{e}/\text{\AA}^3$, smaller than those in ThH_{10} (ThH_9). This indicates that the H–H covalent bonds in ThH_{10} and ThH_9 are strengthened by capturing the interstitial excess electrons of isolated Th frameworks.

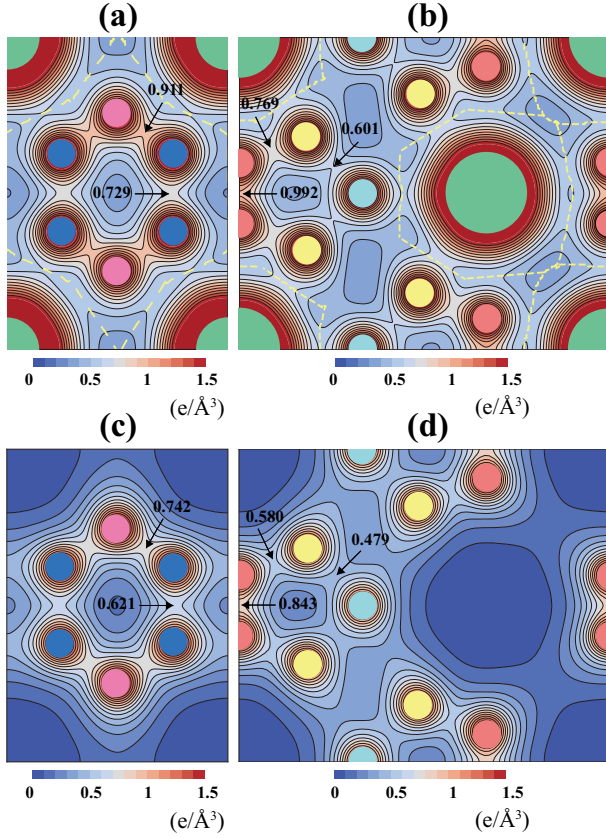


FIG. 5. Calculated total charge densities of (a) ThH₁₀ and (b) ThH₉ at 300 GPa, with a contour spacing of $0.1 e/\text{\AA}^3$. The Bader basins of Th atoms are also drawn in (a) and (b). The calculated charge densities of the isolated H₃₂ and H₂₉ cages of ThH₁₀ and ThH₉ without Th atoms are displayed in (c) and (d), respectively. The numbers represent the values of $\rho_{\text{H-H}}$ at the midpoints (marked by the arrows) of the H-H bonds.

To provide an explanation for the variation of P_c in ThH₁₀, ThH₉, CeH₉, and LaH₁₀, we estimate chemical precompression by calculating the attractive Coulomb forces between a metal atom and its surrounding H atoms [see the lower panel in Figs. 1(a) and 1(b)]. This simple estimation is based on the complete screening of the electric field arising from metal atoms within H cages. Using the Bader [39] analysis, we calculate the cationic charge Q_M inside the Bader basin [see Figs. 5(a) and 5(b)] of metal atom in each superhydride. For ThH₁₀, ThH₉, CeH₉, and LaH₁₀, we obtain Q_M values of 1.486, 1.464, 1.199, and 1.036 e , respectively (see Fig. 6). Assuming that Q_M is the point charge at the position of corresponding metal atom and the anionic charge ($-Q_M$) of H atoms is uniformly distributed on the spherical shell with a radius of $d_{\text{M-H}}$, we evaluate the magnitudes of Coulomb forces acting on the H atoms composing the H₃₂ or H₂₉ cage, and divide it by the surface area of the spherical shell. Figure 6 shows such estimated chemical pressures of ThH₁₀, ThH₉, CeH₉, and LaH₁₀ at 300 GPa, with ratios relative to the value of LaH₁₀. We find that the chemical pressures of ThH₁₀ and ThH₉ (CeH₉) are about two (one and half) times higher than

that of LaH₁₀, indicating that the former Group-4 metal hydrides have larger chemical precompressions to attain lower P_c values than the latter Group-3 metal hydride. Considering that the $d_{\text{M-H}}$ values of ThH₁₀ and ThH₉ are close to that of LaH₁₀ [see Fig. 2(a)], the higher chemical pressures in Th superhydrides are likely attributed to more cationic and anionic charges compared to LaH₁₀. As shown in Fig. 6, the chemical pressures of four superhydrides are well consistent with their variations of Q_M . It is noted that the estimated chemical pressure of CeH₉ is lower than that of isostructural ThH₉ at 300 GPa (see Fig. 6), while the predicted value of $P_c = 100$ GPa for the former is lower than that (110 GPa) for the latter. This inconsistency of chemical precompression and P_c between CeH₉ and ThH₉ may be due to the delocalized nature of Ce 4*f* electrons [46], which could lower P_c via a more hybridization with the H 1*s* state. Nevertheless, despite their crude simulations, the estimated relative chemical pressures of ThH₁₀, ThH₉, CeH₉, and LaH₁₀ are in reasonable agreement with the variation of experimentally measured P_c values [22–27].

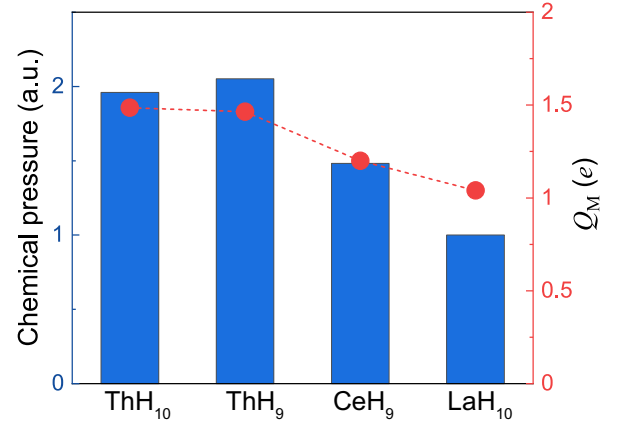


FIG. 6. Calculated chemical pressures of ThH₁₀, ThH₉, CeH₉, and LaH₁₀ at 300 GPa. The cationic charges Q_M of metal atoms obtained from Bader charge analysis are also given.

IV. SUMMARY

Using first-principles DFT calculations, we have conducted a comparative study of chemical precompressions in experimentally synthesized superhydrides including ThH₁₀, ThH₉, CeH₉, and LaH₁₀. We found that these superhydrides form H clathrates by capturing excess electrons in interstitial regions of their isolated fcc- and hcp-metal frameworks. By taking into account the attractive Coulomb interactions between cationic metal atom and its surrounding H atoms, we estimated chemical precompressions in ThH₁₀, ThH₉, CeH₉, and LaH₁₀. It was found that ThH₁₀, ThH₉, and CeH₉ have larger chemical precompressions than LaH₁₀, consistent with the variation of experimentally measured P_c values [22–27]. Our findings not only demonstrated that interstitial excess electrons in the metal frameworks of superhydrides play an

important role in generating the chemical precompression of H cages around metal atoms, but also have important implications for the exploration of new superhydrides which can be synthesized at moderate pressures below ~ 100 GPa.

V. SUPPLEMENTARY MATERIAL

See Supplemental Material for the lattice constants of ThH_{10} , ThH_9 , CeH_9 , and LaH_{10} , the phonon spectrum of ThH_9 , and the valence charge densities of the Th frameworks of ThH_{10} and ThH_9 .

VI. AUTHOR'S CONTRIBUTIONS

S. Y., C. W., and S. L. contributed equally to this work.

VII. ACKNOWLEDGEMENT

This work was supported by the National Research Foundation of Korea (NRF) grant funded by the Korean Government (Grants No. 2019R1A2C1002975, No. 2016K1A4A3914691, and No. 2015M3D1A1070609). The calculations were performed by the KISTI Supercomputing Center through the Strategic Support Program (Program No. KSC-2020-CRE-0163) for the supercomputing application research.

VIII. DATA AVAILABILITY

The data that support the findings of this study are available from the corresponding author upon reasonable request.

* Corresponding author: chojh@hanyang.ac.kr

-
- [1] T. Bi, N. Zarifi, T. Terpstra, and E. Zurek, Reference Module in Chemistry, Molecular Science and Chemical Engineering (Elsevier, New York, 2019).
 - [2] J. A. Flores-Livas, L. Boeri, A. Sanna, G. Profeta, R. Arita, and M. I. Eremets, *Phys. Rep.* **856**, 1 (2020) and references therein.
 - [3] N. W. Ashcroft, *Phys. Rev. Lett.* **21**, 1748 (1968).
 - [4] E. Zurek, R. Hoffmann, N. W. Ashcroft, A. R. Oganov, and A. O. Lyakhov, *Proc. Natl. Acad. Sci. USA* **106**, 42 (2009).
 - [5] Y. Xie, Q. Li, A. R. Oganov, and H. Wang, *Acta Cryst. C* **70**, 104 (2014).
 - [6] J. Hooper and E. Zurek, *J. Phys. Chem. C* **116**, 13322 (2012).
 - [7] H. Wang, J. S. Tse, K. Tanaka, T. Litaka, and Y. Ma, *Proc. Natl. Acad. Sci. USA* **109**, 6463 (2012).
 - [8] D. Duan, Y. Liu, F. Tian, D. Li, X. Huang, Z. Zhao, u. Yu, B. Liu, W. Tian, and T. Cui, *Sci. Rep.* **4**, 6968 (2014).
 - [9] Y. Li, J. Hao, H. Liu, Y. Li, and Y. Ma, *J. Chem. Phys.* **140**, 174712 (2014).
 - [10] X. Feng, J. Zhang, G. Gao, H. Liu, and H. Wang, *RSC Adv.* **5**, 59292 (2015).
 - [11] F. Peng, Y. Sun, C. J. Pickard, R. J. Needs, Q. Wu, and Y. Ma, *Phys. Rev. Lett.* **119**, 107001 (2017).
 - [12] H. Liu, I. I. Naumov, R. Hoffmann, N. W. Ashcroft, and R. J. Hemley, *Proc. Natl. Acad. Sci. USA* **114**, 6990 (2017).
 - [13] Y. Sun, J. Lv, Y. Xie, H. Liu, and Y. Ma, *Phys. Rev. Lett.* **123**, 097001 (2019).
 - [14] H. Xie, Y. Yao, X. Feng, D. Duan, H. Song, Z. Zhang, S. Jiang, S. A. T. Redfern, V. Z. Kresin, C. J. Pickard, and T. Cui, *Phys. Rev. Lett.* **125**, 217001 (2020).
 - [15] L. Liu, C. Wang, S. Yi, K. W. Kim, J. Kim, and J.-H. Cho, *Phys. Rev. B* **99**, 140501(R) (2019).
 - [16] C. Wang, S. Yi and J.-H. Cho, *Phys. Rev. B* **101**, 104506 (2020).
 - [17] A. P. Durajski, R. Szcześniak, Y. Li, C. Wang, and J.-H. Cho, *Phys. Rev. B* **101**, 214501 (2020).
 - [18] C. Heil, S. diCataldo, G. B. Bachelet, and L. Boeri, *Phys. Rev. B* **99**, 220502(R) (2019).
 - [19] Y. Quan, S. S. Ghosh, and W. E. Pickett, *Phys. Rev. B* **100**, 184505 (2019).
 - [20] D. A. Papaconstantopoulos, M. J. Mehl, and P.-H. Chang, *Phys. Rev. B* **101**, 060506(R) (2020).
 - [21] A. P. Drozdov, M. I. Eremets, I. A. Troyan, V. Ksenofontov, and S. I. Shylin, *Nature (London)* **525**, 73 (2015).
 - [22] M. Somayazulu, M. Ahart, A. K. Mishra, Z. M. Geballe, M. Baldini, Y. Meng, V. V. Struzhkin, and R. J. Hemley, *Phys. Rev. Lett.* **122**, 027001 (2019).
 - [23] A. P. Drozdov, P. P. Kong, V. S. Minkov, S. P. Besedin, M. A. Kuzovnikov, S. Mozaffari, L. Balicas, F. F. Balakirev, D. E. Graf, V. B. Prakapenka, E. Greenberg, D. A. Knyazev, M. Tkacz, and M. I. Eremets, *Nature (London)* **569**, 528 (2019).
 - [24] D. V. Semenok, A. G. Kvashnin, A. G. Ivanova, V. Svitlyk, V. Y. Fomin, A. V. Sadakov, O. A. Sobolevskiy, V. M. Pudalov, I. A. Troyan, and A. R. Oganov, *Mater. Today* **33**, 36 (2020).
 - [25] X. Li, X. Huang, D. Duan, C. J. Pickard, D. Zhou, H. Xie, Q. Zhuang, Y. Huang, Q. Zhou, B. Liu, and T. Cui, *Nat. Commun.* **10**, 3461 (2019).
 - [26] N. P. Salke, M. M. Davari Esfahani, Y. Zhang, I. A. Kruglov, J. Zhou, Y. Wang, E. Greenberg, V. B. Prakapenka, J. Liu, A. R. Oganov, and J.-F. Lin, *Nat. Commun.* **10**, 4453 (2019).
 - [27] W. Chen, D. V. Semenok, X. Huang, H. Shu, X. Li, D. Duan, T. Cui, and A. R. Oganov, *arXiv:2101.01315* (2021).
 - [28] P. P. Kong, V. S. Minkov, M. A. Kuzovnikov, S. P. Besedin, A. P. Drozdov, S. Mozaffari, L. Balicas, F. F. Balakirev, V. B. Prakapenka, E. Greenberg, D. A. Knyazev, and M. I. Eremets, *arXiv:1909.10482* (2019).
 - [29] D. Zhou, D. V. Semenok, D. Duan, H. Xie, W. Chen, X. Huang, X. Li, B. Liu, A. R. Oganov, and T. Cui, *Sci. Adv.* **6**, eaax6849 (2020).
 - [30] E. Snider, N. Dasenbrock-Gammon, R. McBride, M. Debessai, H. Vindana, K. Vencatasamy, K. V. Lawler, A. Salamat, and R. P. Dias, *Nature (London)* **586**, 373 (2020).
 - [31] R. P. Dias and I. F. Silvera, *Science* **355**, 715 (2017).
 - [32] P. Loubeyre, F. Occelli, and P. Dumas, *Nature (London)* **577**, 631 (2020).
 - [33] N. W. Ashcroft, *Phys. Rev. Lett.* **92**, 187002 (2004).
 - [34] Z. M. Geballe, H. Liu, A. K. Mishra, M. Ahart, M. Somayazulu, Y. Meng, M. Baldini, and R. J. Hemley, *Angew. Chem., Int. Ed.* **57**, 688 (2018).
 - [35] H. Liu, I. I. Naumov, Z. M. Geballe, M. Somayazulu, J. S. Tse, and R. J. Hemley, *Phys. Rev. B* **98**, 100102(R) (2018).

- [36] C. Wang, S. Yi, and J.-H. Cho, Phys. Rev. B **100**, 060502(R) (2019).
- [37] A. M. Shipley, M. J. Hutcheon, M. S. Johnson, R. J. Needs, and C. J. Pickard, Phys. Rev. B **101**, 224511 (2020).
- [38] S. Yi, C. Wang, H. Jeon, and J.-H. Cho, Phys. Rev. Materials **5**, 024801 (2021).
- [39] R. F. W. Bader, Acc. Chem. Res. **18**, 9 (1985).
- [40] G. Kresse and J. Hafner, Phys. Rev. B **48**, 13115 (1993).
- [41] G. Kresse and J. Furthmüller, Comput. Mater. Sci. **6**, 15 (1996).
- [42] P. E. Blöchl, Phys. Rev. B **50**, 17953 (1994).
- [43] J. P. Perdew, K. Burke, M. Ernzerhof, Phys. Rev. Lett. **77**, 3865 (1996); **78**, 1396(E) (1997).
- [44] L. Kývala and D. Legut, Phys. Rev. B **101**, 075117 (2020).
- [45] P. Giannozzi, S. Baroni, N. Bonini, M. Calandra, R. Car, C. Cavazzoni, D. Ceresoli, G. L. Chiarotti, M. Cococcioni, I. Dabo, *et al.* J. Phys.: Condens. Matter **21**, 395502 (2009).
- [46] H. Jeon, C. Wang, S. Yi, and J.-H. Cho, Sci. Rep. **10**, 16878 (2020).
- [47] I. Errea, F. Belli, L. Monacelli, A. Sanna, T. Koretsune, T. Tadano, R. Bianco, M. Calandra, R. Arita, F. Mauri, and J. A. Flores-Livas, Nature (London) **578**, 66 (2020).
- [48] I. Errea, M. Calandra, C. J. Pickard, J. Nelson, R. J. Needs, Y. Li, H. Liu, Y. Zhang, Y. Ma, and F. Mauri, Phys. Rev. Lett. **114**, 157004 (2015).
- [49] I. Errea, M. Calandra, C. J. Pickard, J. R. Nelson, R. J. Needs, Y. Li, H. Liu, Y. Zhang, Y. Ma, and F. Mauri, Nature (London) **532**, 81 (2016).
- [50] A. P. Durajski, Sci. Rep. **6**, 38570 (2016).
- [51] B. Silvi and A. Savin, Nature (London) **371**, 683 (1994).
- [52] M.-S. Miao and R. Hoffmann, J. Am. Chem. Soc. **137**, 3631 (2015).
- [53] J. Wang, Q. Zhu, Z. Wang, and H. Hosono, Phys. Rev. B **99**, 064104 (2019) and referenes therein.
- [54] Z. Zhao, S. Zhang, T. Yu, H. Xu, A. Bergara, and G. Yang, Phys. Rev. Lett. **122**, 097002 (2019).
- [55] E. Kaxiras, Atomic and Electronic Structure of Solids. (Cambridge University Press, New York, 2003) p. 152.